In Vitro Validation of Viscoelastic and Nonlinear Physical Model of Liver for Needle Insertion Simulation

Yo Kobayashi, *Member, IEEE*, Akinori Onishi, Hiroki Watanabe, Takeharu Hoshi, Kazuya Kawamura,
and Masakatsu G. Fujie, *Member, IEEE*

Abstract— **Needle insertion treatments require accurate placement of the needle tip into the target cancer. However, it is difficult to insert the needle into the cancer because of cancer displacement due to the organ deformation. Then, a path planning using numerical simulation to analyze the deformation of the organ is important for the accurate needle insertion. The objective of our work is to develop and validate a viscoelastic and nonlinear physical liver model. First, an overview is given of the development of the physical liver model. Second, the experimental method to validate the model is explained. In-vitro experiments that made use of a pig's liver were conducted for comparison with the simulation using the model. Results of the in-vitro experiment showed that the liver model reproduces 1) the relationship between needle displacement and force during needle insertion, 2) velocity dependence of needle displacement and force when a puncture occurs, and 3) nonlinear and viscoelastic response of displacement at an internally located point displacement, with high accuracy.**

I. INTRODUCTION

A. Percutaneous therapy and puncture assisting robot

As a cancer treatment method, percutaneous therapy is now a focus of attention. For example, PEIT (Percutaneous Ethanol Injection Therapy) and RFA (Radio Frequency Ablation) are performed for liver cancer. In this form of treatment, cancer cells existing inside the organ are necrotized by delivering a needle tip to the cancer cells in order to either inject ethanol (PEIT) or ablate (RFA). Percutaneous therapy has become a major trend in liver cancer treatment with the benefit of very minimally invasive but sufficient results.

Y. Kobayashi is with Consolidated Research Institute for Advanced Science and Medical Care, Waseda University, Japan, (59-309, 3-4-1, Ohkubo Shinjuku-ku, Tokyo, Japan, phone: +81-3-5286-3412; fax: +81-3-5291 -8269; e-mail: you-k@aoni.waseda.jp).

A. Onishi, H. Watanabe, T. Hoshi and K. Kawamura are with the Graduate School of Science and Engineering, Waseda University, Japan.

M. G. Fujie is with the Graduate School of Science and Engineering, Waseda University, and the Faculty of Science and Engineering, Waseda University, Japan.

In recent years, research and development have been carried out on surgical robots and navigation systems for minimally invasive and precise surgery [1]-[2]. Research into robotic systems to assist needle insertion has also been conducted to improve the accuracy of needle placement and expansion of the approach path. The authors of this paper are also developing robot assisted surgery systems based on the physical organ model shown in Fig. 1 [3]-[7].

B. Physical model of organ

In percutaneous therapy, it is necessary to accurately place the needle tip on the target cancer. Because a target organ such as liver consists of soft tissue, the organ changes its shape (i.e., deforms), which also changes the position of the target lesion. For the reason, it is necessary to devise a plan for the insertion path that takes into account the organ deformation. A numerical simulation in a virtual surgery environment reproduced with physical models of organs may be used to make such a plan. The needle must be accurately directed to the target lesion when puncture occurs, since the needle immediately advances inside the tissue when the needle punctures the liver. Therefore, it is important to make a correct analysis of the organ deformation and set the appropriate conditions where puncture occurs.

Then, a number of research groups have conducted studies on the development of deformable organ model. For example, Alterovitz et al. researched the simulation of steerable needle insertion for prostate brachytherapy [8]-[9]. Meanwhile, DiMaio et al. developed a linear system for analyzing the extent of phantom deformation of planar tissue during needle insertion by using a linear elastic material model [10]-[11]. Moreover, Sakuma et al. show the equation that combines both logarithmic and polynomial strain energy forms of a pig liver from combined compression and elongation tests [12]–[13]. Salcudean et al. showed a planning system to find the optimized insertion angle and position using linear and nonlinear organ models [14]-[15]. Finally, Schwartz et al.
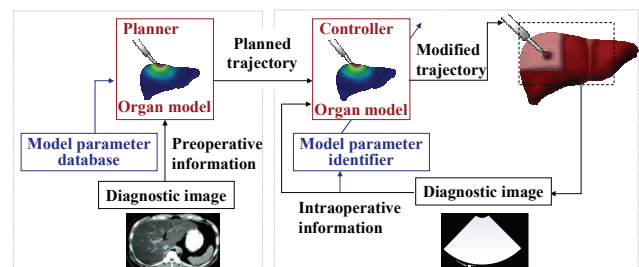

Fig. 1: The needle insertion system based on physical organ model.

present a viscoelastic and nonlinear model for the simulation of needle insertion [16].

In general, tissue modeling is complex because tissue exhibits inhomogeous, nonlinear, anisotropic elastic and viscous behavior [17]. In particular, the viscoelastic and nonlinear properties of tissue are important for precise needle insertion. It has been reported that there is nonlinear relation between the force loaded on the needle and the deformation of the liver deformation [18] as a result of nonlinear properties. It is well known that since the liver has viscoelastic properties, its deformation is dependent on the velocity of needle insertion [19]. For this reason, it is necessary to use models reflecting organ properties such as viscoelasticity and nonlinearity in order to reproduce organ deformations that may occur during needle insertion.

C. Objectives

Our work focused on the development of a model including both viscoelastic and nonlinear properties. Schwartz et al. already present a model including viscoelastic and nonlinear properties[16]. However, the material properties included in that model is coarse approximation of the real material properties of biological soft tissues. The originality of our work is the development of a viscoelastic and nonlinear liver model based on the detailed material properties of tissues. The authors have been investigating a study on the physical model of the liver and reported on a finite element model that reflects the viscoelasticity and nonlinearity properties in previous work [3]-[6].

The purpose of this paper is the validation of the proposed model. More specifically, the following responses of the physical liver model is evaluated and validated:

1) Relationship between needle displacement and force during needle insertion

2) Velocity dependence of needle displacement and force when a puncture occurs

3) Viscoelastic and nonlinear response of the displacement at an internally located point.

This report is organized as follows: Section II presents the simplified explanation of our liver model, including the material properties of the model and the formulation and solution of the FEM-based model. Section III examines the first two responses listed above and compares the data of the real liver and proposed liver model. Section IV compares the displacement data (third response above) of the real liver and proposed model. Section V presents our conclusions and future work.

This paper focuses on the development of a model, including the viscoelastic and nonlinear properties. Then, an accurate setting of the liver shape and boundary conditions will be carried out in future work.

II. PHYSICAL MODEL OF LIVER

A. Material properties

The material properties of a pig liver were both measured and modeled in our experiments. We already reported the material properties of a pig liver in previous papers [3]-[4], in which we also gave specific descriptions of the physical properties of the liver. Thus, only a simplified explanation of the material behavior is shown in this paper.

Experiments were individually conducted to measure the physical properties of the pig's interior liver using a rheometer (TA Instrument Co. : AR550). The shear modulus, shear stress and shear strain were then calculated based on these results. The viscoelastic and nonlinear properties of pig liver are reported in the following.

1) Viscoelastic properties: A dynamic viscoelastic test was carried out to measure the frequency response of the liver. Sine-wave stress from 0.1 to 250 rad/s, providing 3% strain amplitude, was loaded on the liver, and the mechanical impedance of the pig liver was obtained. The result of the dynamic viscoelastic test is shown in Fig. 2. $G*$ is the complex shear modulus, G' is the storage elastic modulus, and G'' is the loss elastic modulus.

In general, the needle is inserted into the organ at low velocity; hence, the response is mainly affected by low-frequency characteristics. Thus, we used the viscoelastic model using the fractional derivative described in (1), which considers only the low-frequency characteristics.

$$G\frac{d^k \gamma}{dt^k} = \tau \qquad (1)$$

where t is time, τ is the shear stress, γ is the shear strain, G is the viscoelasticity, and k is the order of the derivative.

Based on the slope of G' and G'' in Fig. 2, the derivative order k is approximately equal to 0.1.

2) Nonlinear properties (strain dependence of G): The nonlinear characteristics of liver material were investigated with a creep test, in which the step response is measured. The steady state of the step response following sufficient elapsed time exhibits the low-frequency characteristics described in (1). Equation (2) is obtained if (1) is solved by the conditions of the creep test.

$$\gamma = \frac{\tau_c}{G\,\Gamma(1+k)}t^k = \gamma_c t^k \qquad (2)$$

where τ_c is constant shear stress, γ_c is the coefficient deciding the strain value and $\Gamma()$ is the gamma function.

A creep test for each stress of step response was carried out while the viscoelasticity G and strain γ_c for each stress were calculated using (2). Figure 3 shows the viscoelasticity G vs.
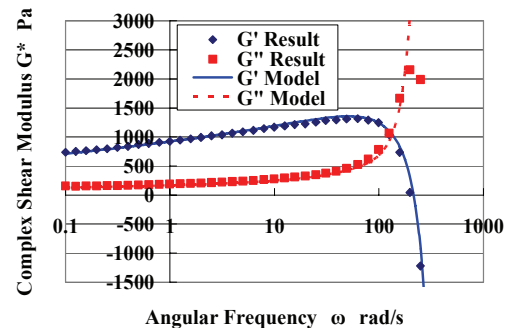
Fig. 2: Mechanical impedance of liver[3]-[4]. G* is the complex shear modulus, G' is the storage elastic modulus, and G" is the loss elastic modulus.

strain γ_c diagram of these results. The experimental result shows a liver with low strain of less than approximately 0.35 displays linear characteristics and a viscoelasticity G at a constant 400 Pa, while a liver with high strain of more than approximately 0.35 displays nonlinear characteristics and an increased degree of viscoelasticity. Then, the strain dependence can be modeled using the quadratic function of strain shown by (3).

$$G(\gamma) = \begin{cases} G_o & (\gamma < \gamma_0) \\ G_0(1 + a_\gamma(\gamma - \gamma_0)^2) & (\gamma > \gamma_0) \end{cases} \quad (3)$$

where G_o is the viscoelastic modulus of the linear part, γ_0 is the strain in which the liver begins to show nonlinearity and a_γ is the coefficient for deciding the change of stiffness.

3) Shear stress-strain relationship: The material properties of the liver are modeled using (4) from the discussions given in 1) and 2).

$$G(\gamma)\frac{d^k\gamma}{dt^k} = \tau \quad (4)$$

4) Stress-strain relationship: In general, elastic modulus E is used to construct the deformation model based on Finite Element Method (FEM). The relation between elastic modulus E and shear modulus G is calculated using Poisson's ratio ν in the following equation.

$$E = 2(1+\nu)G \quad (5)$$

Up to this point of experiments with the rheometer, we have considered only one type of applied stress acting on a liver. Many situations of deformation simulation involve more than one type of stress occurring simultaneously. We assume that the nonlinearity of the elastic modulus is decided by the relative strain calculated in (6).

$$\varepsilon_r = \sqrt{\frac{2}{9}\{(\varepsilon_1 - \varepsilon_2)^2 + (\varepsilon_2 - \varepsilon_3)^2 + (\varepsilon_3 - \varepsilon_1)^2\}} \quad (6)$$

where ε_1, ε_2, ε_3 represent the principal strain.

Thus, the material properties using the liver model are described in (7)-(8).

$$E(\varepsilon_r)\frac{d^k\varepsilon}{dt^k} = \sigma \quad (7)$$

$$E(\varepsilon_r) = \begin{cases} E_o & (\varepsilon_r < \varepsilon_0) \\ E_0(1 + a_\varepsilon(\varepsilon_r - \varepsilon_0)^2) & (\varepsilon_r > \varepsilon_0) \end{cases} \quad (8)$$

where σ is the stress vector, and ε is the strain vector.
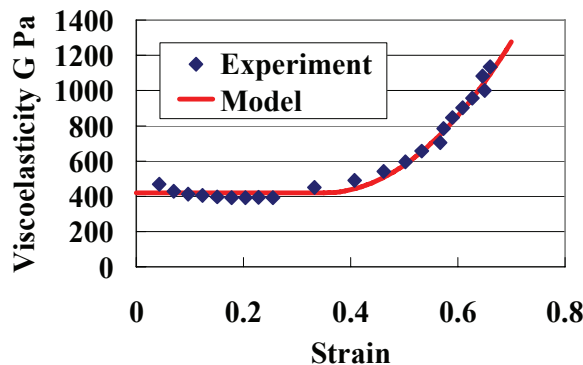

Fig. 3: The viscoelasticity G–strain γ_c diagram [3] -[4]

B. FEM based Modeling

This section displays the FEM model using the material properties shown in Section II-A. We have already reported the formulation and solution to the FEM model in previous papers, which also provide specific descriptions [5]-[6]. Thus, only a simplified explanation is shown in this paper.

The expression of the displacements at all nodal points and all applied loads is written in (9)-(11) from the result of (8).

$$\mathbf{K(U)}D^{(k)}\mathbf{U} = \mathbf{F} \quad (9)$$

$$\mathbf{K(U)} = \sum_{all\ element} \mathbf{k}(\varepsilon_r) \quad (10)$$

$$\mathbf{k}(\varepsilon_r) = \begin{cases} \mathbf{k_0} & (\varepsilon_r < \varepsilon_0) \\ \mathbf{k_0}(1 + a_\varepsilon(\varepsilon_r - \varepsilon_0)^2)(\varepsilon_r > \varepsilon_0) \end{cases} \quad (11)$$

where $\mathbf{k}$ is the nonlinear element stiffness matrix, $\mathbf{k_0}$ is the element stiffness matrix when the liver tissue shows linear characteristics, a_ε is the coefficient deciding the change of stiffness and ε_r is the relative strain.

In the following sections, first, the solution for the viscoelastic system is shown in 1), followed by the solution for the nonlinear system in 2). Finally, the solution for (9) is shown from both discussions 1) and 2).

1) Solution for the viscoelasticitc system: The equation (9) can be considerably simplified when the following conditions are fulfilled [20]:
- The derivative operator of (9) is a common factor in the stiffness of all elements.
- Only the external loads influence the stresses.
Then, equation (12) is derived from (9).

$$\mathbf{K(U)U} = \mathbf{F'} \quad (\mathbf{F'} = D^{(-k)}\mathbf{F}) \quad (12)$$

where $D^{(-k)}$ means the kth-order integration.

Equation (12) is identical to the elastic problem when the virtual external force vector $\mathbf{F'}$ is used. The fractional calculation (12) for each component of external force vector $\mathbf{F}$ is implemented in order to obtain the virtual external force vector $\mathbf{F'}$. We use the sampling time-scaling property introduced in [21] to realize a discrete fractional calculation.

2) Nonlinear system: Incremental approaches are important for obtaining a significant answer because there is no unique answer in many nonlinear situations. The incremental form of the discretized nonlinear model is generally written by (13).

$$\mathbf{K_t(U_n)}\Delta\mathbf{U_n} = \Delta\mathbf{F_n} \quad (13)$$

where $\mathbf{K_t}$ is the tangential stiffness matrix, $\Delta\mathbf{U_n}$ is the increment of the overall displacement vector and $\Delta\mathbf{F_n}$ is the increment of the overall external force. The tangential matrix $\mathbf{K_t}$ is described in (14) from equation (11).

$$\mathbf{K_t(U)} = \sum_{all\ element} \mathbf{k_t}(\varepsilon_r) \quad (14)$$

$$\mathbf{k_t}(\varepsilon_r) = \begin{cases} \mathbf{k_0} & (\varepsilon_r < \varepsilon_0) \\ [1 + a_\varepsilon(\varepsilon_r - \varepsilon_0)^2 + 2a_\varepsilon(\varepsilon_r - \varepsilon_0)\varepsilon_r]\mathbf{k_0} & (\varepsilon_r > \varepsilon_0) \end{cases} \quad (15)$$

where $\mathbf{k_t}$ is the tangential element stiffness matrix, and $\mathbf{k_0}$ is the element stiffness matrix during linear characteristics.

We use both the Euler method and Modified Newton-Raphson method to solve the nonlinear system, as shown in Fig. 4.

3) Calculation process: Based on these discussions, the solution for system (9) is described as follows. First, the virtual external force **F'** is calculated, then the increment of **F'** (**ΔF'**) is computed. The solution to the nonlinear system described in 2) is then carried out using **ΔF'**.

$$K_t(U_n)\Delta U_n = \Delta F'_n \qquad (16)$$

In this section, development of the physical liver model based on FEM was shown. The validation experiment of the proposed model is carried out in the following sections. Section III shows the experimental validation of these model responses: 1) relationship between needle displacement and force during needle insertion and 2) velocity dependence of needle displacement and force when a puncture occurs. Section IV shows the evaluation for the model response of 3) displacement at an internally located point for the purpose of investigating model accuracy to simulate the displacement of cancer.

III. VALIDATION I
- NEEDLE INSERTION FORCE AND VELOCITY DEPENDENCE-

In this section, validation of the proposed liver model about the needle insertion force and velocity dependence of the needle force and displacement where a puncture occurs is described. First, an in vitro experiment using a pig liver is shown. Next, the response of the proposed liver model is simulated. By comparing the measurement data for the experiment and the simulation, we validate the liver model.

A. Methods of in vitro experiments

A needle insertion experiment was conducted on a real pig liver to measure the force applied to the needle and the needle displacement. In addition, several needle insertion experiments were conducted under the same condition so that the variation of experiment data could be obtained. Additional experiments were conducted with different needle insertion velocities to investigate the velocity dependence of the force applied to the needle and the needle displacement when a puncture occurs.

The experiment details are shown as follows, as well as an overview of the measurement experiment in Fig. 5.
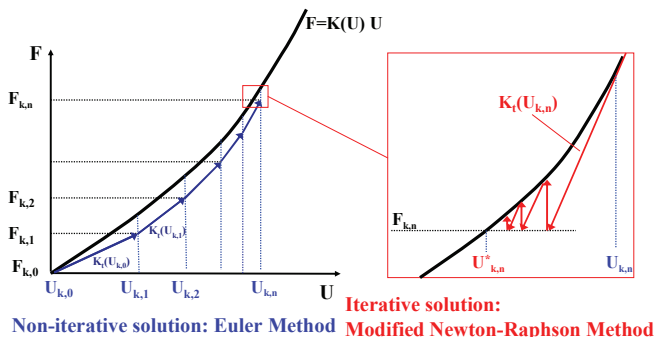

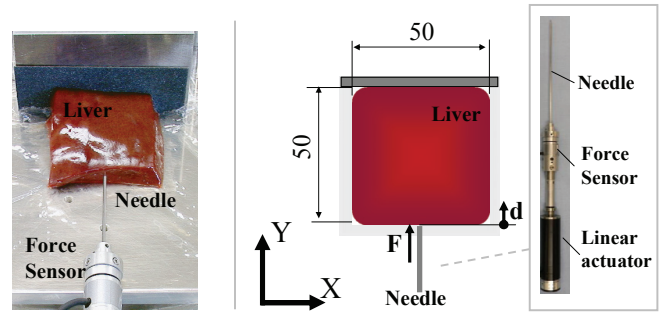Fig. 4: The solution to the nonlinear FEM equation.

Fig. 5: Experimental setup.

1) Liver shape/boundary condition: The liver was cut into a rectangular shape (50 x 50 mm, approx. 20 mm thickness) and placed on the measurement table so that the dorsal aspect of the liver was fixed. When the liver was fixed, double-sided tape was used to place sandpaper on the fixing wall, and then the liver and sandpaper were attached each other with instant glue.

2) Experimental equipment: The needle used in this study was biopsy needles (17 gauge). As shown in Fig. 5, the configuration of the experimental equipment includes a linear actuator with force sensor. The linear actuator enables the realization of a degree of freedom toward the needle insertion, and the force sensor enables the measurement of the force applied to the needle.

3) Experimental conditions: The experiments were conducted with the variations of needle insertion velocity ranging from 0.5 mm to 8 mm. The experimental conditions of needle insertion velocity were set for seven velocities (0.5, 1.0, 2.0, 3.0, 4.0, 6.0, and 8.0) and nine trial experiments were performed for each velocity (total: 63 trials). The experiments were conducted with three parts of the liver removed from a single pig. The force applied to the needle and the needle displacement was measured during experiment.

B. Methods of Simulation

1) Setting boundary condition of the liver: A model with a shape similar to a liver was used in experiment of section III-*A*. The shape of the liver model was a 50 x 50 mm rectangle and the thickness was 20 mm, which was the same as the liver used in the experiment. As boundary conditions, the dorsal side of the model was set as the fixed end. The model shape and boundary conditions are shown in Fig. 6.

Each parameter of the liver model was manually set to correspond with the behavior of the experimental results, as shown in Fig. 7.

2) Simulation conditions: The node at needle contact was forced to displace 10 mm towards the Y axis at 4 mm/s when the simulation was performed. Next, simulations were conducted with variations of the needle insertion velocity ranging from 0.5 mm to 8 mm. The needle displacement where the needle force becomes the average of the puncture force obtained in the experiment (0.32 N: ref. Experimental result of Fig. 8: and III-D.) was measured in each simulation.
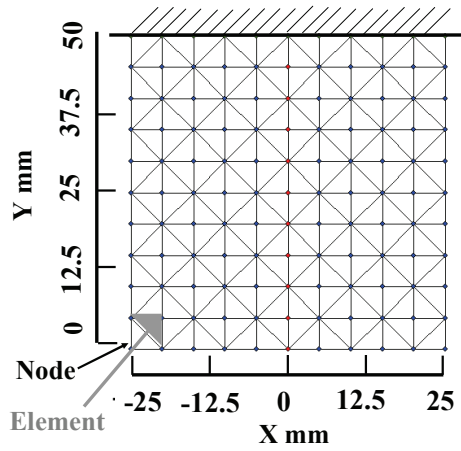
Fig. 6: Boundary condition of the liver model and produced mesh. A 2-D slice of the liver model is defined using mesh triangular elements. The total node number of this model is 121, the total element number is 200, and the model thickness is 20 mm.

C. Results

1) Experiments: Figure 7 shows the relation between the needle displacement and the force applied to the needle during needle insertion. The data in Fig. 7 shows an example when the needle insertion velocity was 4 mm/s. As shown in previous work [18]-[19], the main puncture is designated by a peak in force after a steady rise, followed by a sharp decrease. This data explains that when a needle punctures the liver, it does not keep cutting the tissue with a certain force; instead, 1) it pushes the tissue and then 2) the tissue is punctured instantaneously.

For each set of experimental data, puncture displacement d_c and puncture force F_c were manually extracted and sorted into the each velocity of needle insertion. Figures 8 and 9 show the puncture force and the puncture displacement, respectively, for each needle insertion velocity.

2) Simulations: The simulation result of the relationship between needle displacement and force when the insertion velocity is 4 mm/s is shown in Fig. 7. The result shows the nonlinear relationship between the needle force and displacement. The simulation result of puncture force and displacement at each insertion velocity is shown in Fig. 8 and Fig. 9. Figure 10 shows the deformation result of the physical model of the liver when the insertion velocity is 4 mm/s.

D. Discussion

1) Needle force and displacement: Figure 7 shows the relationship between the needle displacement and force of the real liver and liver model. The result of the experiment displays the nonlinear relationship of the needle displacement and force. It is assumed that this result stems from the nonlinear characteristics of liver, that is, liver subject to high strain displays features of rigidity whereas liver subject to lower strain does not, as shown in Fig.3.

The simulation result also shows the nonlinear relationship; in other words, the liver model reproduces the relationship between needle displacement and force of the liver with high accuracy.
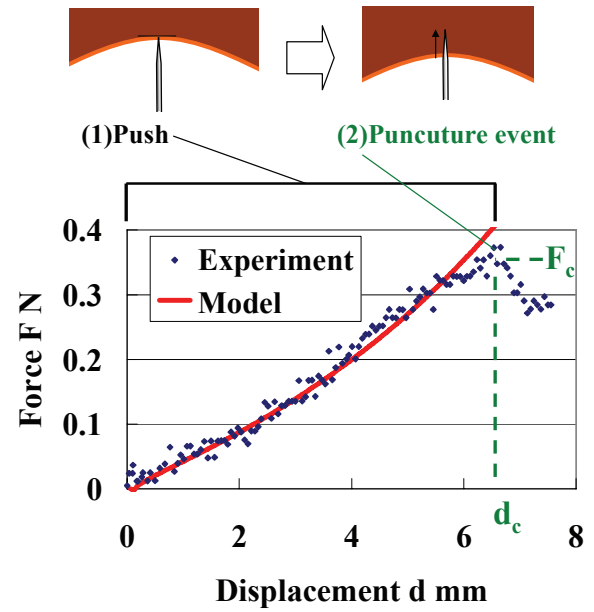

Fig. 7: The force applied to the needle. The blue points represent experimental data, and the red line shows the model response of needle insertion force.
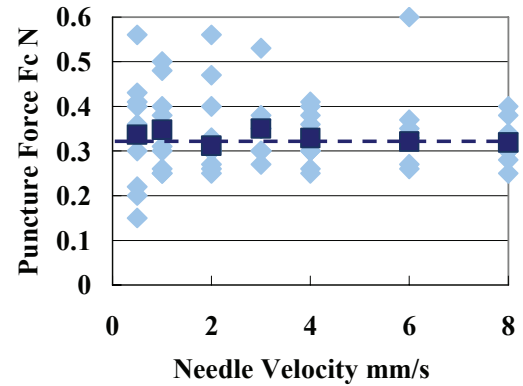

Fig. 8: Relationship between needle velocity and puncture force. Light blue points represent experimental data, and blue points represent the median of each needle insertion velocity.
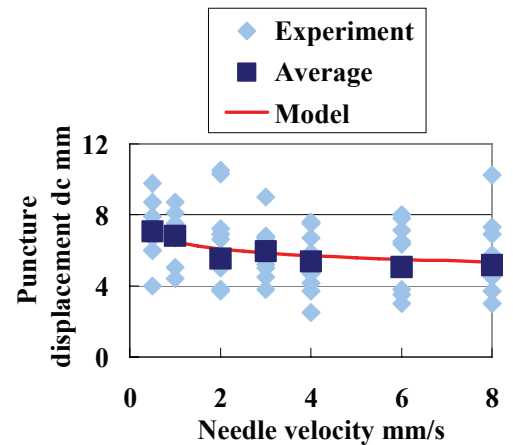

Fig. 9: Relationship between needle velocity and puncture displacement. Light blue points represent experimental data, and blue points represent the median of each needle insertion velocity. The red line shows the model response of needle displacement, where the force loaded on the needle becomes the puncture force (=0.32 N).

(a) Needle displacement 2 [mm]

(b) Needle displacement 4 [mm]
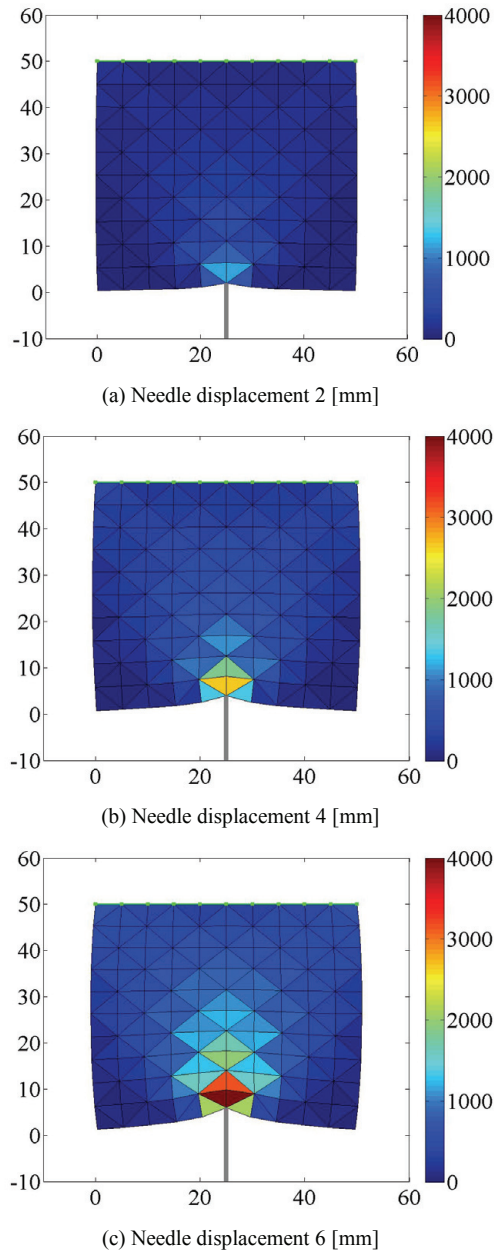

(c) Needle displacement 6 [mm]

Fig. 10: Deformation results of the liver model when insertion velocity is 4 mm/s. The color of each element is the stress Pa.

2) Needle velocity dependence: The following discussions are advanced using the median values shown in Figs. 8 and 9, while variation of the experiment data was obtained. The discussions about variation of the experiment have been discussed in author's previous work [22].

The puncture force has no velocity dependence because it shows almost constant values from the median values of the puncture force displayed in Fig. 8. In contrast, the median values of the puncture displacement in Fig. 9 show that the puncture displacement becomes smaller as the needle insertion velocity increases. It is assumed that this result stems from the viscoelastic characteristics of liver, as shown in Fig.2.

The puncture displacement where the force loaded on the needle becomes the puncture force (0.32 N) at each insertion

velocity, is shown in Fig. 9. The simulation result also shows that the puncture displacement becomes smaller as the needle insertion speed increases, and the liver model reproduces the velocity dependence of the puncture displacement of the liver with high accuracy.

IV. VALIDATION II
- THE DISPLACEMENT AT AN INTERNALLY LOCATED POINT-

In this section, validation of the proposed liver model about 3) the displacement at an internally located point is described. First, the measurement method of the displacement at an internally located point in the real liver is shown. Next, the simulation to measure the displacement of the liver model is displayed. Finally, we validate the proposed model, comparing the measurement data for the real liver and the liver model,

A. Measurement of liver deformation

Some research shows methods for the measurement of organ deformation. For example, DiMaio et al. [10] measured the deformation of a liver or phantom by sensing the displacement of a marker attached to the phantom surface. This method measures the deformation of the liver surface. However, there is a significant difference between the deformation of the liver surface to which the marker is attached, and the deformation of the liver in the needle plane.

In this study, medical ultrasound equipment was used to measure the deformation of the liver in the needle plane. The medical ultrasound equipment was chosen from other diagnostic imaging systems because time-series data is required to validate the viscoelastic properties. The experimental setup and conditions are shown as follows (Fig. 11).

1) Liver shape and boundary condition: The liver was cut into a rectangular solid (60 x 60 mm, thickness 20 mm), and the rear side of the liver was constrained by a wall. The liver was attached to the sandpaper using glue and the sandpaper was attached to the wall using double-sided tape. A dimensional outline drawing of the liver is shown in Fig. 11.

2) Experimental instrument: The experimental setup for the actuator and force sensor was the same as the experiment described in Section III. Part of the wall was perforated and the medical ultrasound equipment was set into the perforated part. This setup avoided the effect of liver deformation caused by the ultrasound probe coming into contact with the liver. The probe of the ultrasound medical equipment was set at the needle plane. Deformation was measured through image recognition of the ultrasound images.

The ultrasound images of the liver include various special features because of the presence of various tissues such as fat. The feature point on the ultrasound image is assumed to be a virtual target that represents the cancer, and pattern recognition (normal correlation) was carried out to measure the position of the virtual target through the use of an image processing computer. The point in the white box in the ultrasound image in Fig. 11 shows the measured point. The initial length between the measured point and the wall is 36 mm.
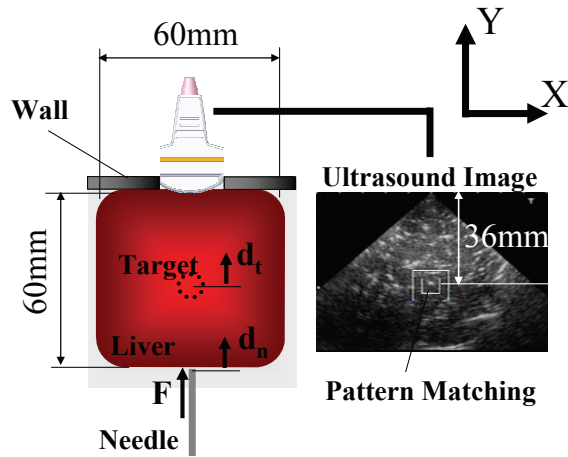
Fig. 11: The experimental setup.

3) Experimental conditions: The needle was inserted from the center of the liver surface (Fig. 11). The axial force loaded onto the needle in the Y direction was controlled to the ordered force, which was set to increases linearly by 0.45 N at 0.025 N/s during the first 18 seconds. Subsequently, the ordered force was set to a constant force at 0.45 N for 30 seconds. In this experiment, the nonlinear property of the liver was evaluated based on the liver's response during linear increase, and the viscoelastic property of the liver was evaluated based on the liver's response during constant force.

The time-series data of needle displacement and displacement of the virtual target was collected during the experiment.

B. Simulation

1) Setting boundary condition of the liver: A 2-D slice of the liver model was defined using triangular mesh elements. The mesh shape was the same as that in the experiment shown in Section III. The stiffness parameters of the model, such as G_o, ε_o and a_ε were set manually to fit the experimental data.

2) Simulation conditions: The needle was assumed to be inserted into the center of the liver model at $(X, Y) = (0, 0)$ mm, and the force was set to load the node at $(0.0, 0.0)$ mm in the Y direction. The ordered force was set to increase linearly by 0.45 N at 0.025 N/s during the first 18 seconds. Subsequently, the ordered force was set to a constant force at 0.45 N for 30 seconds.

The time-series data of the needle displacement and displacement of the virtual target were collected during the experiment. The initial position of the virtual target was set to be the same as the measured point in the experiment, as shown in A.

C. Results

Figure 12 shows the time-series data of the needle displacement and the displacement of the virtual target, measured by experiment A. The time-series data of the needle displacement and displacement of the virtual target on the simulation is also shown in Fig. 12.

D. Discussions

1) Needle displacement (0–18 s): The needle displacement obtained from the experiment in Fig.12 increases linearly when the loaded force is small (0–5 s), but the data when the loaded force is large (5–18 s) show a low rate of increase. It is assumed that this result stems from the nonlinear characteristics of liver, that is, liver subject to high strain displays features of rigidity, as shown in Fig.3.

The result from the simulation also shows a linear increase for a small force (0–5 s) and a low rate of increase of needle displacement when the loaded force is large (5–18 s). Also, Fig. 12 shows that the liver model reproduces the nonlinear response of the real liver with high accuracy.

2) Needle displacement (18–50 s): The needle displacement obtained from experiment increases after the loaded force is set to be constant (18–50 s). It is assumed that this result stems from the viscoelastic characteristics of liver, that is, the strain on the liver increases with constant stress, as shown in equation (2).

The result from the simulation also shows the needle displacement increase during constant force (18–50 s). Thus, Fig. 12 shows that the liver model reproduces the viscoelastic response of the real liver with high accuracy.

3) Displacement of virtual target (0–18 s): The displacement of an internally located virtual target from the experiment increases with acceleration in the early stages of applying a load (0–5 s). (First, the rate of displacement is low, but then the displacement increases rapidly.) Meanwhile, the displacement increases linearly when the loaded force is small (5–15 s), whereas the data when the loaded force is large (15–18 s) show a low increase rate.

The simulation result shows an accelerating increase in Fig. 12, although the simulation result has a 1 mm error in comparison with the data measured by the real organ in the early stage of applying a load (0–5 s), but the error diminishes with the increase of the loaded force. And, the liver model reproduces the nonlinear response of displacement at an internally located point shown in the real liver with high accuracy when the loaded force is considerable (12–18 s).
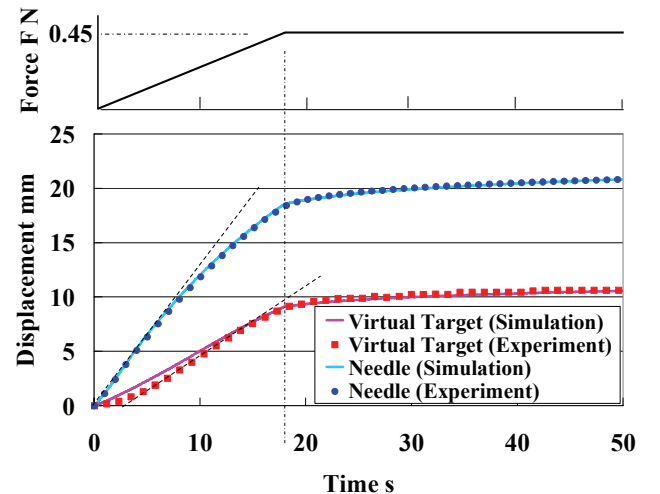

Fig. 12: The Displacement of an internally located virtual target

4) Displacement of virtual target (18–50 s): The displacement of an internally located virtual target from the experiment also increases after the loaded force is set to be constant (18– 50 s).

The result from the simulation also shows the displacement increases during constant force (18–50 s). Thus, Fig. 12 shows that the liver model reproduces the viscoelastic response of displacement at an internally located point shown in the real liver with high accuracy.

V. CONCLUSIONS AND FUTURE WORK

This paper presents the in vitro validation of a physical liver model. First, a simplified explanation of the material behavior and the formulation and solution of the FEM based model are shown. Next, validation experiments are shown. Both in vitro experiments and simulations were carried out to compare the measurement data for the real liver and the liver model. The validation results show that the proposed model reproduces the following nonlinear and viscoelastic responses of the real liver: 1) relationship between needle displacement and force during needle insertion, 2) velocity dependence of needle displacement when a puncture event occurs, and 3) displacement at an internally located point.

In future, further precise liver modeling will be carried out to realize more accurate needle insertion. A liver model should be developed that considers inhomogeneous properties when the target is a liver affected by disease, including hepatic cirrhosis and cancer. And, the accurate setting of liver shape and boundary conditions also will be carried out. First, a liver model with the actual shape and complex boundary conditions of a real pig liver should be validated so it can be used for more detailed evaluations. Then, it should be determined whether the proposed liver model can be generalized to human liver tissue. The model parameter identification method using intra-operative information will also be researched, with reference to the ambiguity of the model parameter. Finally, the organ model-based needle insertion system will be further developed for use in safe and precise clinical treatment.

REFERENCES

[1] R. H. Taylor and D. Stoianovici "Medical Robotics in Computer-Integrated Surgery", IEEE Transactions on Robotics and Automation,Vol. 19, No. 5, pp.765-781,2003

[2] P. Daraio, B. Hannaford and A. Menciassi, "Smart Surgical Tools and Augmenting Devices", IEEE Transactions on Robotics and Automation, Vol. 19, No. 5, pp.782-792,2003

[3] Y. Kobayashi, J. Okamoto, M. G. Fujie "Physical Properties of the Liver for Needle Insertion Control", In IEEE International Conference on Intelligent Robotics and Systems (2004), pp.2960-2966, 2004

[4] Y. Kobayashi, J. Okamoto, M.G. Fujie "Physical Properties of the Liver and the Development of an Intelligent Manipulator for Needle Insertion", In IEEE International Conference on Robotics and Automation (2005), pp.1644-1651,2005

[5] Y. Kobayashi, A. Onishi, T. Hoshi, K. Kawamura and M. G. Fujie, "Viscoelastic and Nonlinear Organ Model for Control of Needle Insertion Manipulator", in Proceeding of the 29th Annual International Conference of the IEEE Engineering in Medicine and Biology Society, pp1242-1248, 2007

[6] Y. Kobayashi, A. Onishi, T. Hoshi, K. Kawamura and M. G. Fujie, "Deformation Simulation using a Viscoelastic and Nonlinear Organ Model for Control of a Needle Insertion Manipulator", in Proceedings of 2007 IEEE International Conference on Intelligent Robots and Systems, pp1801-1808,2007

[7] T. Hoshi, Y. Kobayashi, K. Kawamura, M. G. Fujie, "Developing an Intraoperative Methodology Using the Finite Element Method and the Extended Kalman Filter to Identify the Material Parameters of an Organ Model", in Proceeding of the 29th Annual International Conference of the IEEE Engineering in Medicine and Biology Society, pp.469-474, 2007

[8] R.Alterovitz, A. Lim, K. Goldberg, G. S. Chirikjian, and A. M. Okamura, "Steering Flexible Needles under Markov Motion Uncertainty", In International Conference on Intelligent Robots and Systems (2005), pp120-125,2005

[9] R.Alterovitz, K. Goldberg, and A. Okamura, "Planning for Steerable Bevel-Tip Needle Insertion through 2D Soft Tissue with Obstacles", In IEEE International Conference on Robotics and Automation (2005), pp.1652-1657,2005

[10] S.P.DiMaio and S.E.Salcudean "Needle Insertion Modelling and Simulation", In IEEE Transaction on Robotics and automation,Vol. 19, No. 5, pp864-875, 2003

[11] S.P.DiMaio and S.E.Salcudean "Interactive Simulation of Needle Insertion Model", In IEEE Transaction on Biomedical Engineering,Vol. 52, No. 7, pp.1167-1179, 2005

[12] O. Goksel , S.E. Salcudean, S. P. DiMaio, R. Rohling and J. Morris, "3D Needle-Tissue Interaction Simulation for Prostate Brachytherapy", in Medical Image Computing and Computer-Assisted Intervention (2005), pp.827-834, 2005

[13] E.Dehghan, S.E.Salcudean, "Needle Insertion Point and Orientation Optimization in Non-linear Tissue with Application to Brachytherapy", in 2007 IEEE International Conference on Robotics and Automation, pp.2267-2272, 2007

[14] I. Sakuma, Y. Nishimura, C. K. Chui, E. Kobayashi, H. Inada, X. Chen, and T. Hisada, "In vitro Measurement of Mechanical Properties of Liver Tissue under Compression and Elongation Using a New Test Piece Holding Method with Surgical Glue", Proccedings on International Symposium IS4TM, pp.284-292, 2003

[15] C.Chui, E. Kobayashi, X. Chen, T. Hisada and I. Sakuma, "Combined compression and elongation experiments and non-linear modelling of liver tissue for surgical simulation", Medical and Biological Engineering and Computing. Volume 42, Number 6, pp.787-798, 2006

[16] J.M. Schwartz, M. Denninger, D. Rancourt, C. Moisan and D. Laurendeau. "Modelling liver tissue properties using a non-linear visco-elastic model for surgery simulation", Medical Image Analysis, Volume 9, Issue 2, pp. 103-112, 2005

[17] N.Famaey, J. V. Sloten, "Soft tissue modelling for applications in virtual surgery and surgical robotics" in Computer Methods in Biomechanics and Biomedical Engineering, 11:4, pp.351-366

[18] A.M.Okamura, C.Simone and M.D.O'Leary, "Force modeling for needle insertion into soft tissue", In IEEE Transaction on Biomedical Engineering,Vol. 51, No. 10, pp.1707-1716, 2004

[19] M.Heverly, P.Dupont, J.Triedman,"Trajectory Optimization for Dynamic Needle Insertion", In IEEE International Conference on Robotics and Automation (2005), pp.1646- 1651,2005

[20] O.C. Zienkiewicz and Y.K.Cheung, "The Finite Element Method in Structural and Continuum Mechanics" (1967)

[21] C. Ma and Y. Hori, "The Application of Fractional Order Control to Backlash Vibration Suppression", In Proceedings of American Control Conference (2004), 2901-2906

[22] Y. Kobayashi, A. Onishi, T. Hoshi, K. Kawamura and M. G. Fujie, "Modeling of Conditions where a Puncture Occurs during Needle Insertion considering Probability Distribution", in Proceedings of 2008 IEEE International Conference on Intelligent Robots and Systems, 2008 (submitted)